Superlattices and Microstructures 109 (2017) 480–489

Contents lists available at ScienceDirect

Superlattices and Microstructures

journal homepage: www.elsevier.com/locate/superlattices

Growth of large grain-size $Cu_2ZnSn(S_xSe_{1-x})_4$ thin films by annealing precursors sputtered from a single quaternary target for solar cells application

Gang Yang [a], Yong-Feng Li [a, b, **], Bin Yao [a, b, *], Zhan-Hui Ding [b], Rui Deng [c], Hai-Feng Zhao [d], Li-Gong Zhang [d], Zhen-Zhong Zhang [d]

[a] State Key Lab of Superhard Materials and College of Physics, Jilin University, Changchun, 130023, PR China
[b] Key Laboratory of Physics and Technology for Advanced Batteries (Ministry of Education), College of Physics, Jilin University, Changchun, 130012, PR China
[c] School of Materials Science and Engineering, Changchun University of Science and Technology, Changchun, 130022, PR China
[d] State Key Laboratory of Luminescence and Applications, Changchun Institute of Optics, Fine Mechanics and Physics, Chinese Academy of Sciences, No. 3888 Dongnanhu Road, Changchun, 130033, PR China

ARTICLE INFO

Article history:
Received 2 April 2017
Received in revised form 15 May 2017
Accepted 16 May 2017
Available online 17 May 2017

Keywords:
CZTSSe
Sputtering
Quaternary target
Se supply
Solar cell

ABSTRACT

A simple and cost effective method of sputtering a single quaternary target following a rapid thermal process (RTP) was applied to prepare $Cu_2ZnSn(S_xSe_{1-x})_4$ (CZTSSe) thin films. The different Se supply during thermal annealing was used to adjust the Se contents in films. The structure, morphology, optical and electrical properties of the CZTSSe films were analyzed comprehensively. Polycrystalline kesterite CZTSSe absorbers with large columnar grains were obtained. The grains are densely packed and surfaces are smooth. The evolution of the optical and electrical properties with different Se contents in the CZTSSe films was studied in details. The conversion efficiency of the Se-rich CZTSSe thin film solar cell was determined to be 3.38%, and the corresponding J-V characteristic was analyzed carefully. The severe interface recombination is the key factor for the large ideality factor and reverse saturation current.

1. Introduction

Kesterite-based $Cu_2ZnSn(S_xSe_{1-x})_4$ (CZTSSe) is a potential absorber material for thin film photovoltaic devices [1]. It has a suitable and tunable band gap (E_g) of 1–1.5 eV with a various Se content. The CZTSSe with a thickness of few microns can absorb nearly all the photons with energy higher than E_g due to its high absorption coefficient larger than 10^4 cm^{-1} [2,3]. Furthermore, constituent metals are non-toxic and abundant on the earth's crust compared with CdTe and $Cu(In,Ga)Se_2$ (CIGS) [4]. Considerable efforts have been devoted to fabricate CZTSSe based solar cells [5–8], the record efficiency of 12.6% has been achieved by hydrazine based solution approaches [9]. In addition, efficiencies over 10% were also obtained by thermal co-evaporation [10], magnetron sputtering [11] and spray deposited methods [12]. These results demonstrate that CZTSSe thin films have great potential in large-scale thin film photovoltaic applications.

* Corresponding author. State Key Lab of Superhard Materials and College of Physics, Jilin University, Changchun, 130023, PR China.
** Corresponding author. State Key Lab of Superhard Materials and College of Physics, Jilin University, Changchun, 130023, PR China.
E-mail addresses: liyongfeng@jlu.edu.cn (Y.-F. Li), binyao@jlu.edu.cn (B. Yao).

http://dx.doi.org/10.1016/j.spmi.2017.05.036
0749-6036/

Among various physical and chemical deposition approaches, magnetron sputtering technology has advantages in depositing uniform films on a large area. Meanwhile, this method avoids the use of poisonous organic solvents and reduces the pollution [13]. Compared with the multi-target sputtering approach widely used, sputtering a single quaternary target using one power source is the simplest and cost effective method [14]. This promising method has been successfully applied in the fabrication of CIGS solar cells. It has also been extensively investigated for the preparation of CZTS thin films recently [15–19]. Solar cells with efficiencies of 6.48% and 4.04% have been obtained by sulfuring the precursors sputtered from a CZTS target, but the use of toxic H_2S gas limits its application in commercial production [20,21]. It has been reported that an efficiency of 2.85% was obtained by using less toxic S powders as the S source during the annealing process [22]. Recently, Feng et al. also obtained a device with the efficiency of 4.4% via sulfurizing the CZTS precursors with S powders [23]. However, all these solar cells utilized the pure CZTS. The relatively low crystal quality and the large bandgap of the pure CZTS might be not conducive to obtain high efficiencies.

There is now a broad consensus that large grains are essential for accomplishing high-efficiency solar cells. Ideally-large grains extended parallel to the substrate in the absorber are expected to reduce the grain boundaries and defects. Therefore, the recombination rate of the photo-generated electron decrease and the minority carrier diffusion length increase in polycrystalline thin film solar cells. In addition, owing to the trade-off effect of the bandgap on the open circuit voltage (V_{oc}) and short circuit current (J_{sc}), most of the reported high-efficiency solar cells have the absorbers with a bandgap of around 1.12 eV. Hence, the bandgap engineering is an important way to maximize the light absorption and ensure optimal V_{oc}. For CZTSSe compound, its bandgap decreases with the increase of Se content, in other words, films with high Se contents are expected. However, in a conventional slow selenization process, S atoms are usually fully replaced by Se, leading to an extremely low bandgap. But in a rapid thermal process, Se contents can be precisely tuned by altering the ratio of $S/(S + Se)$ in the annealing atmosphere due to the short cycle time for reaction. Furthermore, the crystalline quality of the films improved significantly after a rapid thermal process [24–26]. Se elements can also promote the growth of grains and reduce the grain boundaries. In addition, Chen et al. declared that more facile n-type and p-type doping in high Se content CZTSSe films is beneficial for achieving high-efficiencies [27].

In this work, we report on the single-step sulfo-selenization of the CZTS precursor sputtered from a quaternary target. A simple rapid thermal process capable of adjusting the bandgap as well as decreasing the recombination rate in the bulk is of interest. It should be noted that S and Se powders were used instead of the toxic H_2S/H_2Se. The influence of different Se supply on the structure, morphology, composition, optical and electrical properties has been studied. Furthermore, a CZTSSe thin film solar cell fabricated with the Se-rich film shows an efficiency of 3.38% and J-V characteristic was studied carefully.

2. Experimental details

2.1. Preparation of CZTS precursor thin films

CZTS precursor films were deposited on soda-lime glass (SLG) substrates by sputtering a quaternary target. The target was fabricated through hot pressed sintering, the detailed process can be found in our previous work [28]. Substrates (2×2 cm^2) were cleaned with acetone, alcohol and demonized water. The vacuum chamber was evacuated to below 7.5×10^{-4} Pa before deposition process. The distance between the target and the substrates was fixed at 60 mm. During the whole process, high-purity argon flow with 30 sccm was introduced as the working gas. The working pressure was kept at 0.1 Pa. The sputtering power for the quaternary target was 60 W and lasted for 60 min to obtain a desired thickness.

2.2. Single-step sulfo-selenization of the CZTS precursor thin films

After sputtering, precursors were annealed by a rapid thermal process. Samples were placed in a graphite box together with 60 mg Se and/or S powders. The quality of S/Se powders was adjusted for realizing the different Se supply. Four samples were labeled as A, B, C and D corresponding to the $S/(S + Se)$ ratio of 1, 2/3, 1/3 and 0, respectively. A three-step heating curve was used. First, the CZTS films were heated to 250 °C and held for 5 min. This preheating step was used to prevent the peeling of the films considering the rapid heating rate of 5 °C/s [29]. Second, to avoid the loss of Zn and Sn elements at higher temperature [30,31], the same heating rate was used to reach a medium temperature 400 °C, heat preservation time for this step was 10 min. Then the final annealing temperature was raised to 560 °C and was also maintained 10 min to guarantee sufficient time for the growth of grains. Finally, samples were cooled down to room temperature by opening the furnace cover.

2.3. Device fabrication

To fabricate solar cells with a typical structure, CZTS precursors were deposited on the Mo-coated SLG substrates (Mo layer with a thickness about 1 μm was deposited by DC sputtering) and annealed using the aforementioned method. The deposition of 50 nm thick CdS buffer layer on the absorber was completed by the chemical bath deposition (CBD) method. Then 50 nm of i-ZnO and 300 nm of ITO were sputtered as the window layers and subsequent the Al grid top electrode was evaporated on the ITO layer. Finally, the devices were mechanically scribed into 9 small cells, the active area of the cell is 0.19 cm^2.

2.4. Characterization

The structure properties of the films were analyzed through an X-ray diffractometer (XRD) with Cu K_α radiation source. Raman scattering of the samples were recorded by a Renishaw micro-Raman spectrometer coupled with a 532-nm excitation laser. The effective penetration depths were estimated to be several hundred nanometers. The morphology and the thickness of the films were characterized by a Hitachi S4800 scanning electron microscope (SEM) and elemental compositions were obtained using an energy dispersive X-ray spectroscope system (EDAX Genesis 2000). An ultraviolet–visible spectrophotometer was used to record the optical absorption spectra of these films. Hall Effect measurement was used to measure the electrical properties of the samples. Current density–voltage (J–V) characterizations were performed under simulated AM1.5G illuminations to determine the efficiency of the CZTSSe based solar cells.

3. Results and discussion

3.1. Analysis of the CZTS target and the sputtered precursor films

The phase purity of the CZTS target is crucial to obtain high-quality precursor films, the quaternary target and the sputtered precursor films were examined firstly. Fig. 1 (a) shows the XRD diffractograms of the target and CZTS precursors. For the CZTS target, almost all the diffraction peaks are related to the kesterite CZTS (PDF Card #26-0575), the absence of second phases indicates that the starting materials reacted during the hot press and synthesized to single phase CZTS. For the precursor films, only two peaks at the position of 28.3° and 58.6°which assigned to (112) and (224) crystal planes can be detected. These samples show a very strong (112) orientation preference. However, the pure CZTS phase cannot be identified just by these two peaks since some binary and ternary chalcogenides share similar crystal structures [32]. Raman detection is needed for further confirmation. As shown in Fig. 1(b), only a main peak at 337 cm^{-1} and a weak peak at 285 cm^{-1} were observed, these peaks are assigned to the Raman shifts of kesterite CZTS [33]. No significant indication of phase separation implying that samples are single phase. The wide peaks of the precursor films indicating the bad crystalline quality of the precursors.

3.2. Composition analysis

The chemical compositions of the target, precursor films and the annealed films were listed in Table 1. The measurement was carried out at different positions and the average values were used. In addition, the standard deviations were also listed in the parenthesis and marked in Italic. It has been reported that high conversion efficiencies can be obtained with Cu poor and slightly Zn rich CZTSSe films [1,9,34]. Therefore, the composition of the CZTS target was designed as Cu/(Zn + Sn) = 0.88 and Zn/Sn = 1.20, respectively. The deficiency of S element is due to the volatilization during the hot press process. Unfortunately, the Zn percentages in the precursor films are much lower than that of the target, which is attributed to the different sputtering yield of each element and the evaporation of Zn. A sublimation of Zn is also likely to happen under frequent bombardment of Ar^+ toward the target [20].

The results for the annealed CZTSSe were also depicted in Fig. 2 for clarity. When the quality of Se powders increases from 0 mg to 60 mg, the contents of S in the films decrease whereas the Se contents change in an opposite way, this implies the successful replacement of S by Se atoms during the heat treatment. This single-step sulfo-selenization of the CZTS precursor was able to obtain CZTSSe films with a large range of S/(S + Se) ratios, but the total contents of the chalcogen are constant. In addition, this treatment may remedy the deficiency of S elements in the target. We also found that there were no dramatic

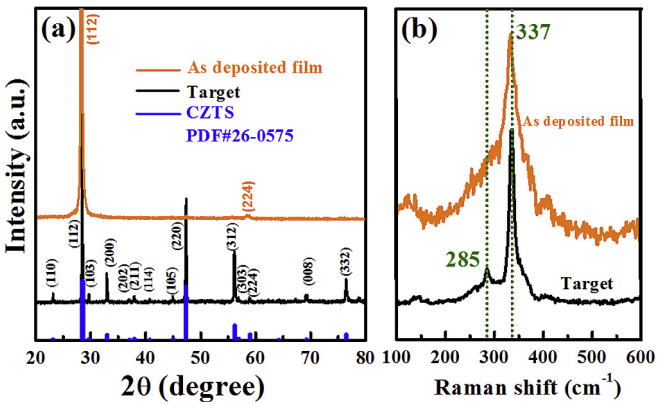

Fig. 1. (a) XRD patterns of the prepared CZTS quaternary target and film deposited on the SLG substrate at 500 °C without annealing. (b) Raman spectroscopic results of the CZTS quaternary target and the as deposited film.

Table 1
Chemical compositions of the CZTS target, the sputtered films, and the annealed CZTSSe films determined by EDS analysis. The values in the parenthesis are the standard deviations.

Sample	Cu	Zn	Sn	S	Se	Cu/(Zn + Sn)	Zn/Sn
Target	25.66*(0.36)*	15.87*(0.36)*	13.22*(0.22)*	45.28*(0.21)*	–	**0.88**	**1.20**
As grown	24.49*(0.63)*	12.40*(0.49)*	14.53*(0.43)*	48.60*(0.30)*	–	**0.91**	**0.85**
A	24.87*(0.60)*	13.21*(0.54)*	13.66*(0.05)*	48.25*(0.24)*	–	**0.93**	**0.97**
B	22.95*(0.38)*	12.03*(0.29)*	13.29*(0.36)*	40.25*(0.85)*	11.48*(1.87)*	**0.91**	**0.91**
C	23.10*(0.18)*	12.60*(0.99)*	13.24*(0.48)*	33.26*(0.68)*	17.81*(2.20)*	**0.89**	**0.95**
D	23.52*(1.62)*	12.15*(0.63)*	13.11*(0.80)*	8.86*(0.74)*	43.12*(2.94)*	**0.93**	**0.93**

The values in bold are the atomic ratios of the metallic elements.

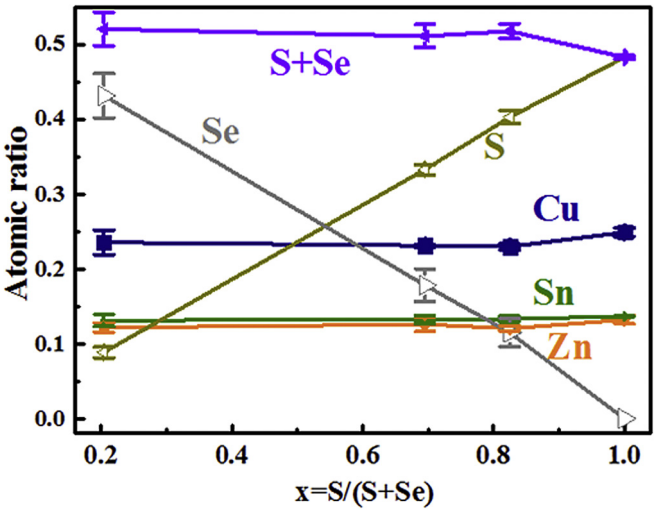

Fig. 2. EDS composition analyses for the annealed films with different Se supply.

changes of metal contents, the constant values of metallic elements enable the discussion about the influence of the different Se supply, because the effect of other point defects can be ruled out.

3.3. Structural studies

3.3.1. XRD analysis

Fig. 3 (a) presents the XRD patterns of the annealed CZTSSe films with various Se contents, peaks marked with the symbol of ● are due to the diffraction of CZTSSe phase [35]. The emergence of some weak peaks reveals the improved crystalline

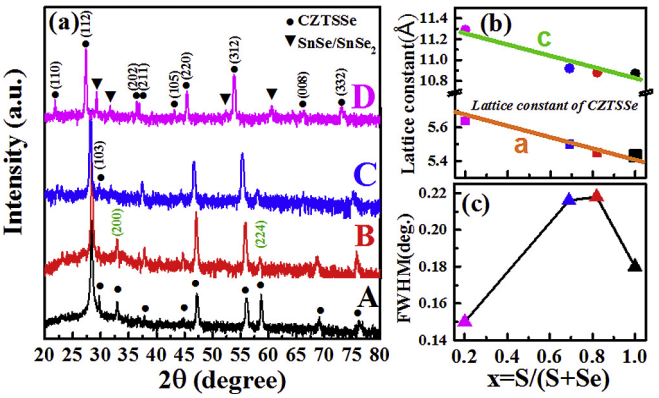

Fig. 3. (a) XRD patterns of the CZTSSe films annealed with different Se supply. A: S/(S + Se) = 1 B: S/(S + Se) = 2/3 C: S/(S + Se) = 1/3 D: S/(S + Se) = 0, (b) The calculated lattice constants from the XRD patterns and (c) The FWHM of (112) diffraction peaks.

quality of CZTSSe films after the rapid thermal annealing. For the films with S/(S + Se) ratio of 0 (i.e., Sample D that subjected to the selenization), the peaks marked by ▼ may be due to the diffraction of SnSe and/or $SnSe_2$ considering that the excess Sn in the films may react with the Se vapor under high temperature. The dominant diffraction peaks of CZTSSe move to lower diffraction angle side regularly as Se contents increase, the shifts are ascribed to the increase of the lattice parameters. For the tetragonal CZTSSe, the relationship between the lattice constants (a and c) and interplanar spacing (d) is:

$$d = \frac{a}{\sqrt{h^2 + k^2 + l^2\left(\frac{a^2}{c^2}\right)}} \quad (1)$$

(h, k, l) are the miller index of the crystal planes. The values of d for (112) and (220) planes can be obtained by the formula: $2d\sin\theta = \lambda$, λ is the wavelength of the Cu K_α radiation, the values of θ can be obtained by fitting the peak positions in XRD patterns. As shown Fig. 3(b), XRD-derived lattice constants (a and c) of CZTSSe films increase linearly with the Se contents, revealing that S^{2-} [r (S^{2-}) = 1.84 Å of effective ionic radius] can be easily replaced by Se^{2-} [r (Se^{2-}) = 1.98 Å] to form CZTSSe solid solutions. The similar variation of these lattice parameters for $CuIn(S,Se)_2$ has also been reported [36]. But it should be noted that S atoms can't be completely replaced by Se even in the selenized sample due to the short reaction time in a rapid thermal process. Furthermore, the intensities of the (200) and (224) diffraction peaks decrease as the Se content increase in CZTSSe films, this variation tendency is similar to the previous results and should be ascribed to the difference of atomic scattering factor [37,38]. Fig. 3(c) plots the values of the full width at half maximum (FWHM) deduced from the (112) peaks. As shown, samples annealed in pure S and pure Se atmosphere (i.e. sample A and sample D) have better crystal quality due to the smaller values of FWHM. However, films grew in mixed S and Se vapor show degraded crystallinity based on their bigger FWHM values. The degraded crystallinity is due to the disordered crystal structure which may come from the random distribution of anions in the lattice [37,39].

3.3.2. *Raman spectroscopy*

Raman spectroscopy is essential to confirm the absence of secondary phases since some impurity phases have the similar crystal structure. Fig. 4 presents the Raman spectra of CZTSSe layers with various S/(S + Se) ratios. For the CZTS film with S/(S + Se) ratio of 1 (sample A), a dominant Raman peak at 337 cm^{-1} and a small peak at 286 cm^{-1} belonging to A_1 mode of CZTS compounds were observed. Hence, the single CZTS phase is confirmed. High intensity and the small FWHM of the dominant Raman peak also imply the formation of high quality CZTSSe thin film [40]. As to the sample B and C contain some Se element, the Raman peaks shift slightly toward lower wavenumber direction. The bimodal behavior and a noticeable peak broadening imply the formation of CZTSSe phase [1,37,41]. The Raman spectrum of sample D (the Se-rich sample) were fitted using the Lorentzian method, three peaks located at 170, 191 and 230 cm^{-1} can be observed in the inset of Fig. 4, these peaks are attributed to CZTSSe phase. It is worth noting that the second phases detected in XRD patterns were not found here due to the small amount of these impurity phases.

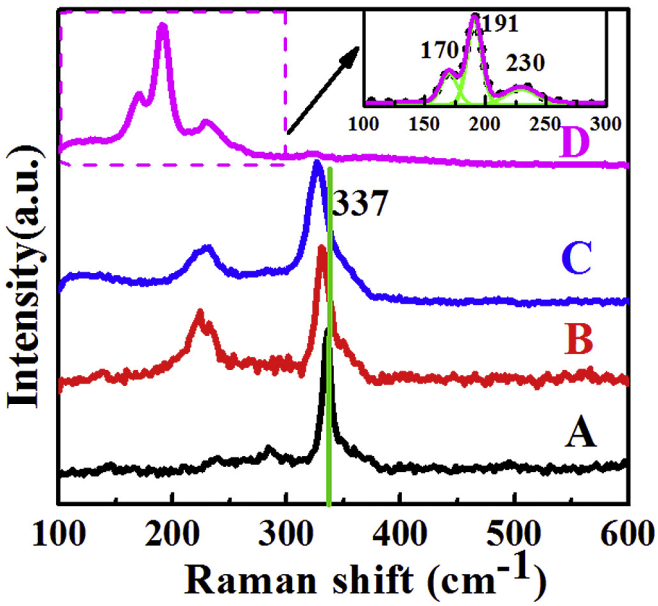

Fig. 4. Raman spectra of CZTSSe thin films annealed with different Se supply. A: S/(S + Se) = 1 B: S/(S + Se) = 2/3 C: S/(S + Se) = 1/3 D: S/(S + Se) = 0. The inset shows the peak fitting results for sample D using Lorentzian method.

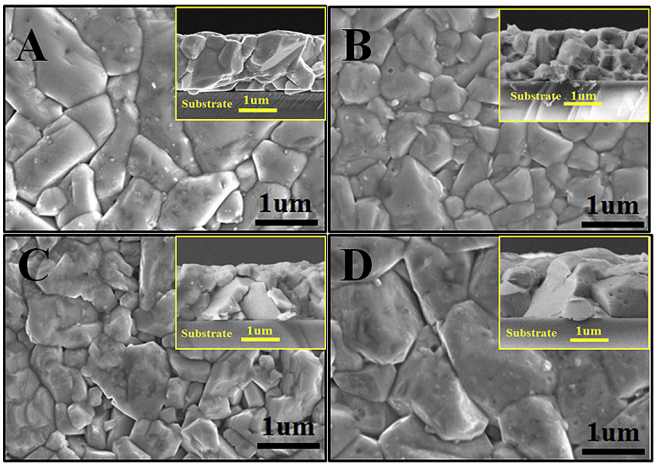

Fig. 5. SEM surface images of the annealed CZTSSe thin films with different Se supply. The insets are the corresponding cross-sectional SEM images of the films. (A:S/(S + Se) = 1 B: S/(S + Se) = 2/3 C: S/(S + Se) = 1/3 D: S/(S + Se) = 0.).

3.3.3. *Film morphology*

The top-view and cross-sectional SEM images of the CZTSSe absorbers with different Se contents were shown in Fig. 5. As shown in the pictures, the crystallinity improved obviously after a rapid thermal process. All the films are void free and have densely packed large grain morphologies. The grain sizes in the sample A and D are more than 2 μm. But the grains are more uniform in sample D because that the Se element can promote the growth of grains [42]. However, the dislocation of Se and S

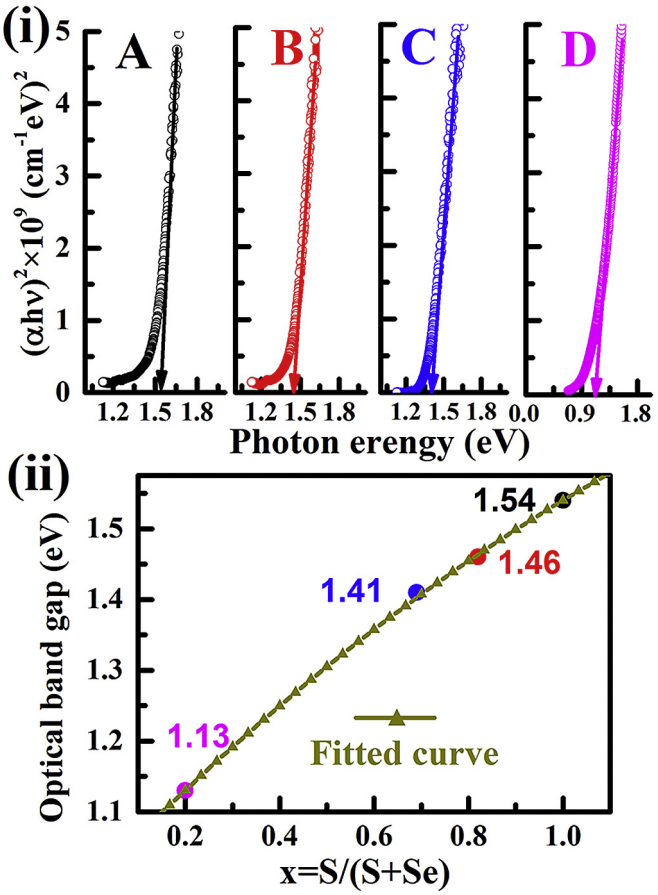

Fig. 6. (a) Plot of $(\alpha h\nu)^2$ vs. photon energy (hν) of the annealed CZTSSe thin films with different Se supply. (b) Dependence of the optical bandgap of CZTSSe alloy films on the Se content.

atoms leads to the crystallization quality decline for sample B and C, for instance, films are composed of much smaller grains. The insets of Fig. 5 show the cross-sectional pictures, films are adhered well with the glass substrates without voids at the interfaces, large columnar grains extended parallel through the film with the thickness about 2 μm. Such characters are favorable to decrease the amount of grain boundaries and diminish recombination in the bulk of the absorber [42–44]. Hence, sample D (S-poor and Se-rich) is more appropriate for photovoltaic application than the other films judging from the morphology.

3.4. Optical properties

As we all know, the V_{oc} is proportional to the bandgap of the absorbers while smaller bandgap broadens the wavelength range of light absorption. Therefore, a bandgap about 1.12 eV should be expected for high performance solar cells. Optical absorption measurements for the annealed films were performed to investigate the dependence of the bandgaps on the different Se supply. As shown in Fig. 6(a), the bandgaps of the four CZTSSe films are 1.54, 1.46, 1.41, and 1.13 eV, respectively. The bandgaps decrease monotonously with the increase of Se contents in the samples as depicted in Fig. 6 (b). The decrease of bandgaps is related to the variation of the hybridization when different amount of Se atoms were introduced [27]. Fit the obtained data using the formula:

$$E_g(x) = (1-x)E_g(CZTS) + xE_g(CZTSe) + bx(1-x) \quad (2)$$

A small bandgap bowing constant ($b \approx 0.13$ eV) can be deduced [45]. The results presented above clearly demonstrate that the bandgap of the CZTSSe thin films can be adjusted via controlling the ratio of S/(S + Se) in the annealing atmosphere. In this experiment, sample D that subjected to the selenization has an optimal bandgap.

3.5. Electrical properties

Electrical properties of the absorbers are very important for p-n junction solar cells. Hall measurements were performed for the CZTSSe films and the results were listed in Table 2. All CZTSSe layers exhibit p-type conducting behaviors because a large number of Cu vacancies (V_{Cu}) serve as acceptors in these films. The carrier concentrations increase significantly with higher Se content. First, The Se p level is higher than that of S, thus the valence-band maximum (VBM) of the selenides is higher, the energy level of the acceptor becomes shallower in Se-rich samples [46]. Second, the compensation of acceptor defects due to the existence of deep donor defects (S vacancies, V_S) also leads to the decrease of carrier concentrations [38,47]. The mobility is an important factor that influences the transport property for the carriers, the carrier mobility for Se-rich CZTSSe and the pure CZTS were 0.556 and 8.08 $cm^2\ V^{-1}\ s^{-1}$, respectively. It is known that the mobility (μ) can be expressed by the equation $\mu = \frac{q\tau}{m^*}$, where q, τ, m^* represents the electronic charge, mean free time of carriers and the effective mass of carriers. The incorporation of Se element results in a weaker restriction of the electrons due to Se atoms has lower electronegativity than S atoms. Therefore, the weaker internal force results in a smaller effective mass (m^*) in Se rich samples [38]. On the other hand, the obtained uniform large grains also contribute to the increase of the mean free time of carriers. Therefore, Se-rich CZTSSe films with large carrier mobility are benefit for the carrier transport.

3.6. Device characterization

Solar cells with a conventional structure were fabricated based on the obtained CZTSSe thin films. The J-V curve for the Se-rich device measured under AM1.5G illuminations was shown in Fig. 7(a). The inset shows the cross-sectional SEM image of the corresponding device. The highest efficiency obtained is 3.38%, the open circuit voltage (V_{oc}), short circuit current density (J_{sc}) and the fill factor (FF) are 320 mV, 30.72 mA/cm^2, and 34.4% respectively. Obviously, the extremely low V_{oc} and FF should be responsible for the unsatisfactory PCE. The analysis of the J–V curve is necessary for better understanding. Based on the solar cell theory, the J–V equation can be expressed as:

$$J = J_{sc} - J_0\left(e^{\frac{q(V-JR_s)}{nkT}} - 1\right) - (V - JR_s)G_{sh} \quad (3)$$

Table 2
Electrical properties of the annealed CZTSSe films that with different Se contents.

Sample	Resistivity (Ω cm)	Carrier Density (cm^{-3})	Hall Mobility ($cm^2V^{-1}s^{-1}$)	Type
A	4.01×10^4	2.52×10^{14}	0.556	p
B	1.12×10^4	4.17×10^{14}	1.57	p
C	277	2.16×10^{16}	1.04	p
D	12.6	6.00×10^{16}	8.08	p

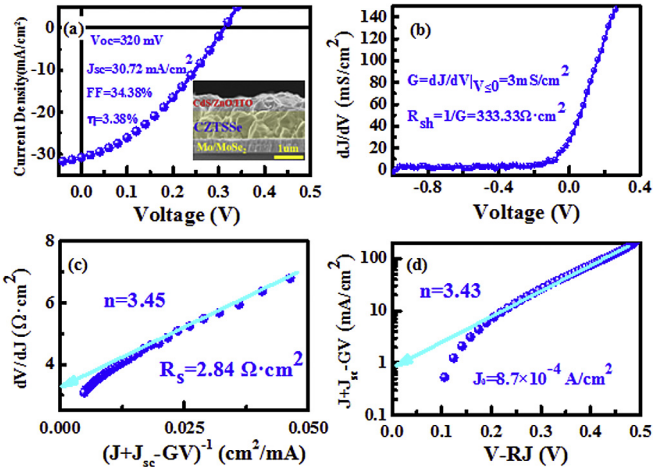

Fig. 7. (a) J–V curves of CZTSSe solar cells measured under AM 1.5G illuminations. Inset: the cross-sectional SEM image of the fabricated CZTSSe cell. (b) Plots of dJ/dV vs V redrawn from the J–V curves. (c) Pots of dV/dJ vs $(J + J_{sc}\text{-}GV)^{-1}$ (d) Semi-logarithmic plots of $J + J_{sc}$–GV vs V–RJ; J_0 was obtained by the intercept of the linear region of the curves, and the slope is equal to q/nkT.

The diode parameters can be obtained by redrawing the J–V curve in three successive plots as shown in Fig. 7 (b), (c) and (d). The values of shunt resistance (R_{sh}), series resistance (R_s), ideality factor (n) and the reverse saturation current density (J_0) were calculated to be 333.33 Ω cm^2, 2.84 Ω cm^2, 3.45 and 8.7 × 10^{-4} A/cm^2, respectively. Using the obtained parameters and the equation:

$$G_{sh}V_{oc} = J_{sc} - J_0\left(e^{\frac{qV_{oc}}{nkT}} - 1\right) \tag{4}$$

The V_{oc} was calculated to be 318.85 mV, which is very close to the measured value (320 mV), indicating that the calculated parameters are credible. The inferior V_{oc} and FF may be due to the contribution of n and J_0. In order to confirm this conclusion, we suppose J = 0 and G_{sh} = 0 in the equation (3), then this equation can be rewritten as:

$$V_{oc} = \frac{nkT}{q}\ln\left(\frac{J_{sc} + J_0}{J_0}\right) \approx \frac{nkT}{q}\ln\frac{J_{sc}}{J_0} \tag{5}$$

Using the values obtained above, the V_{oc} was calculated to be 319.45 mV. Therefore, the V_{oc} is mainly affected by n and J_0. The value of n is much higher than 2 indicates that the interface recombination is the dominated, in other words, the recombination in the bulk of the absorber can be ignored, and this is consistence with the results of morphologies and the Hall measurements. The severe interface recombination may come from the high-density interface defects or tunneling enhanced recombination. Therefore, the large value of J_0 which is mainly attributed to the above-mentioned recombination leads to a relatively low V_{oc}. In addition, Kassis et al. demonstrated that the large values of J_0 and n is one of the major causes for the loss of fill factor [48]. IBM group also reported the improvement of the FF for their CZTSSe devices with the decrease of J_0 and n [49]. In addition, large values of R_s due to the thick $Mo(S,Se)_2$ layer may also influence the FF. Therefore, further research should be focused on improving the quality of the diodes. The high-quality absorber and buffer films with fewer defects as well as an excellent heterojunction with low density interface states are expected to reduce the carrier recombination rate in solar cells.

4. Conclusions

The CZTSSe absorbers were prepared by sputtering a single quaternary target followed by a rapid thermal process. The different Se supply during the annealing was used to adjust the S/(S + Se) ratios in the CZTSSe films. The results of XRD and Raman spectroscopy confirm that Se atoms are easily incorporated into the films to form kesterite CZTSSe. The films with smooth surfaces and densely packed columnar grains were obtained. The optical bandgaps decrease almost linearly with the increase of Se contents. All the CZTSSe films show the p-type conductive behaviors. A Se-rich CZTSSe solar cell with an efficiency of 3.38% has been achieved. The low V_{oc} and FF are attributed to the severe interface recombination. These results show that this method is a simple process to fabricate high quality CZTSSe films with an appropriate bandgap. High efficiency solar cells are expected by further optimization of the interfaces in the devices.

Acknowledgements

This work is supported by the National Natural Science Foundation of China under Grant Nos. 10874178, 11074093, 61205038, 11274135 and 61505067, Specialized Research Fund for the Doctoral Program of Higher Education under Grant No. 20130061130011, Ph.D. Programs Foundation of Ministry of Education of China under Grant No. 20120061120011, and National Found for Fostering Talents of Basic Science under grant No. J1103202. The Science and Technology Development Project of Jilin Province under grant No. 20170101142JC. This work was also supported by Graduate Innovation Fund of Jilin University (No. 2016058).

References

[1] D.B. Mitzi, O. Gunawan, T.K. Todorov, K. Wang, S. Guha, The path towards a high-performance solution-processed kesterite solar cell, Sol. Energy Mater. Sol. Cells 95 (2011) 1421–1436.
[2] F. Jiang, S. Ikeda, T. Harada, A. Ide, A. Mochihara, K. Yoshino, M. Matsumura, Fabrication of an efficient electrodeposited Cu_2ZnSnS_4-based solar cells with more than 6% conversion efficiency using a sprayed Ga-doped ZnO window layer, RSC Adv. 4 (2014) 24351.
[3] Z.Y. Xiao, B. Yao, Y.F. Li, Z.H. Ding, Z.M. Gao, H.F. Zhao, L.G. Zhang, Z.Z. Zhang, Y.R. Sui, G. Wang, Influencing mechanism of the selenization temperature and time on the power conversion efficiency of $Cu_2ZnSn(S,Se)_4$-Based solar cells, ACS Appl. Mater. Interfaces 8 (2016) 17334–17342.
[4] F. Liu, S. Shen, F. Zhou, N. Song, X. Wen, J.A. Stride, K. Sun, C. Yan, X. Hao, Kesterite Cu_2ZnSnS_4 thin film solar cells by a facile DMF-based solution coating process, J. Mater. Chem. C 3 (2015) 10783–10792.
[5] G. Yang, Y.-F. Li, B. Yao, Z.-H. Ding, R. Deng, J.-M. Qin, F. Fang, X. Fang, Z.-P. Wei, L. Liu, Band alignments at interface of Cu_2ZnSnS_4/ZnO heterojunction: an X-ray photoelectron spectroscopy and first-principles study, J. Alloys Compd. 628 (2015) 293–297.
[6] H. Katagiri, K. Jimbo, S. Yamada, T. Kamimura, W.S. Maw, T. Fukano, T. Ito, T. Motohiro, Enhanced conversion efficiencies of Cu_2ZnSnS_4-Based thin film solar cells by using preferential etching technique, Appl. Phys. Express 1 (2008) 041201.
[7] C.K. Miskin, W.-C. Yang, C.J. Hages, N.J. Carter, C.S. Joglekar, E.A. Stach, R. Agrawal, 9.0% efficient Cu2ZnSn(S,Se)4 solar cells from selenized nanoparticle inks, Prog. Photovolt. Res. Appl. 23 (2015) 654–659.
[8] J. Tao, J. Liu, L. Chen, H. Cao, X. Meng, Y. Zhang, C. Zhang, L. Sun, P. Yang, J. Chu, 7.1% efficient co-electroplated Cu_2ZnSnS_4 thin film solar cells with sputtered CdS buffer layers, Green Chem. 18 (2016) 550–557.
[9] W. Wang, M.T. Winkler, O. Gunawan, T. Gokmen, T.K. Todorov, Y. Zhu, D.B. Mitzi, Device characteristics of CZTSSe thin-film solar cells with 12.6% efficiency, Adv. Energy Mater. 4 (2014) 1301465.
[10] Y.S. Lee, T. Gershon, O. Gunawan, T.K. Todorov, T. Gokmen, Y. Virgus, S. Guha, $Cu_2ZnSnSe_4$Thin-Film solar cells by thermal Co-evaporation with 11.6% efficiency and improved minority carrier diffusion length, Adv. Energy Mater. 5 (2015) 1401372.
[11] J. Li, H. Wang, M. Luo, J. Tang, C. Chen, W. Liu, F. Liu, Y. Sun, J. Han, Y. Zhang, 10% Efficiency $Cu_2ZnSn(S,Se)_4$ thin film solar cells fabricated by magnetron sputtering with enlarged depletion region width, Sol. Energy Mater. Sol. Cells 149 (2016) 242–249.
[12] G. Larramona, S. Levcenko, S. Bourdais, A. Jacob, C. Choné, B. Delatouche, C. Moisan, J. Just, T. Unold, G. Dennler, Fine-tuning the Sn content in CZTSSe thin films to achieve 10.8% solar cell efficiency from spray-deposited water-ethanol-based colloidal inks, Adv. Energy Mater. 5 (2015) 1501404.
[13] S.G. Haass, M. Diethelm, M. Werner, B. Bissig, Y.E. Romanyuk, A.N. Tiwari, 11.2% efficient solution processed kesterite solar cell with a low voltage deficit, Adv. Energy Mater. 5 (2015) 1500712.
[14] J. He, L. Sun, K. Zhang, W. Wang, J. Jiang, Y. Chen, P. Yang, J. Chu, Effect of post-sulfurization on the composition, structure and optical properties of Cu_2ZnSnS_4 thin films deposited by sputtering from a single quaternary target, Appl. Surf. Sci. 264 (2013) 133–138.
[15] D. Yoo, M. Choi, S.C. Heo, D. Kim, C. Chung, C. Choi, Rf-magnetron sputtered kesterite Cu_2ZnSnS_4 thin film using single quaternary sputtering target prepared by sintering process, J. Nanosci. Nanotechnol. 13 (2013) 7734–7740.
[16] P. Fan, J. Zhao, G.-X. Liang, D. Gu, Z.-H. Zheng, D.-P. Zhang, X.-M. Cai, J.-T. Luo, F. Ye, Effects of annealing treatment on the properties of CZTSe thin films deposited by RF-magnetron sputtering, J. Alloys Compd. 625 (2015) 171–174.
[17] S.H. Jung, R. Fan, W.I. Lee, C.W. Chung, Structural and electrical properties of radio frequency magnetron sputtered $Cu(In_xGa_{1-x})Se_2$ thin films with additional post heat treatment, Thin Solid Films 547 (2013) 86–90.
[18] H. Kong, J. He, X. Meng, L. zhu, J. Tao, L. Sun, P. Yang, J. Chu, Influence of Se supply for selenization of $Cu(In,Ga)Se_2$ precursors deposited by sputtering from a single quaternary target, Mater. Lett. 118 (2014) 21–23.
[19] L. Ouyang, D. Zhuang, M. Zhao, N. Zhang, X. Li, L. Guo, R. Sun, M. Cao, $Cu(In,Ga)Se_2$ solar cell with 16.7% active-area efficiency achieved by sputtering from a quaternary target, Phys. Status Solidi A 212 (2015) 1774–1778.
[20] M. Xie, D. Zhuang, M. Zhao, Z. Zhuang, L. Ouyang, X. Li, J. Song, Preparation and characterization of Cu_2ZnSnS_4 thin films and solar cells fabricated from quaternary Cu-Zn-Sn-S target, Int. J. Photoenergy 2013 (2013) 1–9.
[21] H. Katagiriand K. Jimbo. Development of rare metal-free CZTS-based thin film soalr cells. in Proceedings of the 37th IEEE Photovoltaic Specialists Conference, (2011) 3516–3521.
[22] J. He, L. Sun, Y. Chen, J. Jiang, P. Yang, J. Chu, Cu_2ZnSnS_4 thin film solar cell utilizing rapid thermal process of precursors sputtered from a quaternary target: a promising application in industrial processes, RSC Adv. 4 (2014) 43080–43086.
[23] J. Feng, X. Huang, W.Z. Chen, J.Y. Wu, H.D. Lin, Q.J. Cheng, D.Q. Yun, F.Y. Zhang, Fabrication and characterization of Cu_2ZnSnS_4 thin films for photovoltaic application by low-cost single target sputtering process, Vacuum 126 (2016) 84–90.
[24] G. Wang, W. Zhao, Y. Cui, Q. Tian, S. Gao, L. Huang, D. Pan, Fabrication of a $Cu_2ZnSn(S,Se)_4$ photovoltaic device by a low-toxicity ethanol solution process, ACS Appl. Mater. Interfaces 5 (2013) 10042–10047.
[25] F. Liu, F. Zeng, N. Song, L. Jiang, Z. Han, Z. Su, C. Yan, X. Wen, X. Hao, Y. Liu, Kesterite $Cu_2ZnSn(S,Se)_4$ solar cells with beyond 8% efficiency by a sol-gel and selenization process, ACS Appl. Mater. Interfaces 7 (2015) 14376–14383.
[26] Y. Yang, X. Kang, L. Huang, S. Wei, D. Pan, A general water-based precursor solution approach to deposit earth abundant $Cu_2ZnSn(S,Se)_4$ thin film solar cells, J. Power Sources 313 (2016) 15–20.
[27] S. Chen, A. Walsh, J.-H. Yang, X.G. Gong, L. Sun, P.-X. Yang, J.-H. Chu, S.-H. Wei, Compositional dependence of structural and electronic properties of $Cu_2ZnSn(S,Se)_4$ alloys for thin film solar cells, Phys. Rev. B 83 (2011).
[28] G. Yang, Y.F. Li, B. Yao, Z.H. Ding, R. Deng, X. Fang, Z.P. Wei, Alternative spectral photoresponse in a p-Cu_2ZnSnS_4/n-GaN heterojunction photodiode by modulating applied voltage, ACS Appl. Mater. Interfaces 7 (2015) 16653–16658.
[29] Y. Lin, S. Ikeda, W. Septina, Y. Kawasaki, T. Harada, M. Matsumura, Mechanistic aspects of preheating effects of electrodeposited metallic precursors on structural and photovoltaic properties of Cu_2ZnSnS_4 thin films, Sol. Energy Mater. Sol. Cells 120 (2014) 218–225.
[30] S. Ahmed, K.B. Reuter, O. Gunawan, L. Guo, L.T. Romankiw, H. Deligianni, A high efficiency electrodeposited Cu_2ZnSnS_4 solar cell, Adv. Energy Mater. 2 (2012) 253–259.
[31] J.J. Scragg, T. Ericson, T. Kubart, M. Edoff, C. Platzer-Björkman, Chemical insights into the instability of Cu_2ZnSnS_4 films during annealing, Chem. Mater. 23 (2011) 4625–4633.
[32] A.C. Lokhande, K.V. Gurav, E. Jo, C.D. Lokhande, J.H. Kim, Chemical synthesis of Cu_2SnS_3 (CTS) nanoparticles: a status review, J. Alloys Compd. 656 (2016) 295–310.

[33] P.A. Fernandes, P.M.P. Salomé, A.F. da Cunha, Growth and Raman scattering characterization of Cu_2ZnSnS_4 thin films, Thin Solid Films 517 (2009) 2519–2523.
[34] A. Fairbrother, X. Fontané, V. Izquierdo-Roca, M. Placidi, D. Sylla, M. Espindola-Rodriguez, S. López-Mariño, F.A. Pulgarín, O. Vigil-Galán, A. Pérez-Rodríguez, E. Saucedo, Secondary phase formation in Zn-rich $Cu_2ZnSnSe_4$ based solar cells annealed in low pressure and temperature conditions, Prog. Photovolt. Res. Appl. 22 (2014) 479–487.
[35] Z.-Y. Xiao, Y.-F. Li, B. Yao, Z.-H. Ding, R. Deng, H.-F. Zhao, L.-G. Zhang, Z.-Z. Zhang, Significantly enhancing the stability of a Cu_2ZnSnS_4 aqueous/ethanol-based precursor solution and its application in $Cu_2ZnSn(S,Se)_4$ solar cells, RSC Adv. 5 (2015) 103451–103457.
[36] T. Wada, H. Kinoshita, Preparation of $CuIn(S,Se)_2$ by mechanochemical process, Thin Solid Films 480–481 (2005) 92–94.
[37] M. Tsega, D.-H. Kuo, Characterization and electrical property of the Cu-deficient $Cu_2ZnSn(S,Se)_4$ bulks at different sulfur contents, J. Alloys Compd. 557 (2013) 142–146.
[38] Y. Dong, J. He, J. Tao, L. Sun, P. Yang, J. Chu, Influence of different S/Se ratio on the properties of $Cu_2Sn(S_xSe_{1-x})_3$ thin films fabricated by annealing stacked metal precursors, J. Mater. Sci. Mater. Electron. 26 (2015) 6723–6729.
[39] O.P. Singh, N. Vijayan, K.N. Sood, B.P. Singh, V.N. Singh, Controlled substitution of S by Se in reactively sputtered CZTSSe thin films for solar cells, J. Alloys Compd. 648 (2015) 595–600.
[40] M.Y. Valakh, O.F. Kolomys, S.S. Ponomaryov, V.O. Yukhymchuk, I.S. Babichuk, V. Izquierdo-Roca, E. Saucedo, A. Perez-Rodriguez, J.R. Morante, S. Schorr, I.V. Bodnar, Raman scattering and disorder effect in Cu_2ZnSnS_4, Phys. Status Solidi RRL 7 (2013) 258–261.
[41] M. Altosaar, J. Raudoja, K. Timmo, M. Danilson, M. Grossberg, J. Krustok, E. Mellikov, $Cu_2Zn_{1-x}Cd_xSn(Se_{1-y}S_y)4$solid solutions as absorber materials for solar cells, Phys. Status Solidi A 205 (2008) 167–170.
[42] M. Dimitrievska, A. Fairbrother, R. Gunder, G. Gurieva, H. Xie, E. Saucedo, A. Perez-Rodriguez, V. Izquierdo-Roca, S. Schorr, Role of S and Se atoms on the microstructural properties of kesterite $Cu_2ZnSn(S_xSe_{1-x})_4$ thin film solar cells, Phys. Chem. Chem. Phys. PCCP 18 (2016) 8692–8700.
[43] H. Guo, Y. Cui, Q. Tian, S. Gao, G. Wang, D. Pan, Significantly enhancing grain growth in $Cu_2ZnSn(S,Se)_4$Absorber layers by insetting Sb_2S_3, $CuSbS_2$, and $NaSb_5S_8$ thin films, Cryst. Growth Des. 15 (2015) 771–777.
[44] M. Johnson, S.V. Baryshev, E. Thimsen, M. Manno, X. Zhang, I.V. Veryovkin, C. Leighton, E.S. Aydil, Alkali-metal-enhanced grain growth in Cu_2ZnSnS_4 thin films, Energy Environ. Sci. 7 (2014) 1931–1938.
[45] M. Bär, W. Bohne, J. Röhrich, E. Strub, S. Lindner, M.C. Lux-Steiner, C.H. Fischer, T.P. Niesen, F. Karg, Determination of the band gap depth profile of the penternary $Cu(In_{(1-X)}\ Ga_X)(S_YSe_{(1-Y)})_2$ chalcopyrite from its composition gradient, J. Appl. Phys. 96 (2004) 3857.
[46] H.-S. Duan, W. Yang, B. Bob, C.-J. Hsu, B. Lei, Y. Yang, The role of sulfur in solution-processed $Cu_2ZnSn(S,Se)_4$ and its effect on defect properties, Adv. Funct. Mater. 23 (2013) 1466–1471.
[47] T. Maeda, S. Nakamura, T. Wada, First principles calculations of defect formation in in-free photovoltaic semiconductors Cu_2ZnSnS_4 and $Cu_2ZnSnSe_4$, Jpn. J. Appl. Phys. 50 (2011) 04DP07.
[48] A. Kassis, M. Saad, Fill factor losses in ZnO/CdS/$CuGaSe_2$ single-crystal solar cells, Sol. Energy Mater. Sol. Cells 80 (2003) 491–499.
[49] T.K. Todorov, J. Tang, S. Bag, O. Gunawan, T. Gokmen, Y. Zhu, D.B. Mitzi, Beyond 11% efficiency: characteristics of state-of-the-art $Cu_2ZnSn(S,Se)_4$Solar cells, Adv. Energy Mater. 3 (2013) 34–38.